

Journal of Materials Chemistry B

Accepted Manuscript



This is an *Accepted Manuscript*, which has been through the Royal Society of Chemistry peer review process and has been accepted for publication.

Accepted Manuscripts are published online shortly after acceptance, before technical editing, formatting and proof reading. Using this free service, authors can make their results available to the community, in citable form, before we publish the edited article. We will replace this *Accepted Manuscript* with the edited and formatted *Advance Article* as soon as it is available.

You can find more information about *Accepted Manuscripts* in the [Information for Authors](#).

Please note that technical editing may introduce minor changes to the text and/or graphics, which may alter content. The journal's standard [Terms & Conditions](#) and the [Ethical guidelines](#) still apply. In no event shall the Royal Society of Chemistry be held responsible for any errors or omissions in this *Accepted Manuscript* or any consequences arising from the use of any information it contains.



Journal Name

ARTICLE

New Imaging Reagents for Lipid Dense Region in Live cells and Nucleus in Fixed MCF-7 cells

Vadde Ramu,^a Firoj Ali,^a Nandaraj Taye,^b Bikash Garai,^a Aftab Alam,^b Samit Chattopadhyay^{*b} and Amitava Das^{*a}

Received 00th January 20xx,
Accepted 00th January 20xx

DOI: 10.1039/x0xx00000x

www.rsc.org/

Two new Uracil (U) and 5-fluorouracil (5-FU) labeled Ruthenium(II)-polypyridyl based cellular imaging reagents are reported. Confocal laser scanning microscopic images with live and paraformaldehyde (PFA) fixed MCF-7 cells are examined using these two low-cytotoxic reagents. Experimental results show that these two complexes, appropriately functionalized with U (**1**) and 5-FU (**2**), have specific affinity for the lipid dense regions like endoplasmic reticulum, cell membrane, and cytoplasmic vacuoles in live MCF-7 cells and dye internalization in these regions happened following an endocytosis pathway. Interestingly, these two complexes are found to be localized in the nucleus of the PFA fixed cells. For fixed cell, presumably the lipid layer disruption helped in the explicit localization of the complexes **1** and **2** in cell nucleus through specific interaction with cellular DNA. Poor and non-specific internalization of an analogous model complex **3**, without having U or 5-FU moiety, reveals the definite influence of U or 5-FU as well as the role of lipophilicity of the respective complex **1** and **2** for the cellular internalization process. Apart from these, large Stokes shift (~160 nm) and appreciably long lived ³MLCT excited state (~320 ns) in aq. buffer medium (pH 7.4) are other key features for complexes **1** and **2**. Unlike the common nuclear DNA staining reagents like DAPI, these low-cytotoxic reagents are found to be highly stable towards photo-bleaching on irradiation with 455 nm at the MLCT band for these complexes.

Introduction

Non-invasive imaging approach is generally preferred for observing individual events in cells compared to the traditional biochemical methods that give average results for cells exposed to certain experimental treatment for studying cell functioning, evolution, differentiation, reproduction, and also gene expression in living organisms.¹ Such processes are expected to affect the native intracellular processes while the imaging studies are performed in physiologically authentic environments and have relevance for cell/molecular biology, studying bio-chemical processes, medicine, pharmacology and diagnostics.² Accordingly, visualization of cellular structure by fluorescence microscopy remains a powerful research tool in recent years. There are significant activities in designing appropriate imaging reagent for visualization of specific organelles with organelle-selective dyes in the membrane-enclosed intracellular structures, as this helps in gaining insight for monitoring important biological processes.^{3,4} Stability towards photo-bleaching, cell membrane permeability,

nominal cytotoxicity and luminescence in the longer wavelength following excitation with non-harmful visible light are some of the essential criteria for any such efficient imaging reagent.⁵⁻⁸ For imaging application, target like ER, a specific organelle in the cells of eukaryotic organisms, has of great significance.^{9,10} Proteins for the secretory pathway are inserted into the membrane of the ER, where they are processed/folded into their native conformation. Misfolded proteins are retained in the ER and transported to the cytosol for ER-associated protein degradation, which has a serious implication in physiology.¹⁰ ER can be stained with a variety of commercially available lipophilic probes and typical highly ER specific dyes include the lipophilic carbocyanine (DiOC6 or DiOC5 with Stokes shift ($\Delta\lambda$ Ss) of ~14 nm) or boron-dipyrromethane (BODIPY) dyes (E34251 or E34250 with $\Delta\lambda$ Ss of ~28 & 7 nm, respectively).¹¹ Such dyes suffer from the limitations of narrow $\Delta\lambda$ Ss, photo-bleaching, and partial toxicity.¹² There are only two reports, which reveal that the above referred limitations could be addressed for either ER or mitochondria-specific dyes by using dinuclear Ru(II)-polypyridyl based complexes.¹³ Gill et al. also showed that the DNA groove-binding dinuclear complex $[\{\text{Ru}(\text{phen})_2\}_2\{-\mu\text{-tpphz}\}]^{4+}$ (where tpphz = tetrapyrrophenazine) could be used to image nuclear DNA in eukaryotic cells,¹⁴ while the 4,7-diphenyl-1,10-phenanthroline (DIP) analogue $[\{\text{Ru}(\text{DIP})_2\}_2\{-\mu\text{-tpphz}\}]^{4+}$ was localised in ER.¹⁵ To the best of our knowledge,

^a Organic Chemistry Division, National Chemical Laboratory, Pune, India, 411008. E-mail: a.das@ncl.res.in.

^b Chromatin and Disease Laboratory, National Center for Cell Science, Pune, India, 411007. E-mail: samit@nccs.res.in.

†Electronic Supplementary Information (ESI) on CLSM images for complex **3** and the x-ray structural details available. See DOI: 10.1039/x0xx00000x

barring these two publications, there is no such report for ER-specific Ru(II)polypyridyl-based imaging reagent for live mammalian cells. It has been argued that lipophilicity of the dye molecule is crucial for ER-specific dye.¹⁶ A recent report also reveals that Ru(II)-polypyridyl-peptide conjugated with lower lipophilicity is preferentially localized in nucleus.^{17,18} All the above referred Ru(II)- and some Ir(III)-based ER-specific dyes are known to induce the toxicity by ER stress and the IC50 values for these reagents are typically $\leq 150 \mu\text{M}$ which defies the suitability of using such reagent for application as an imaging reagent.^{19–22}

We report herein two new and easily accessible uracil (**1**) or 5-fluorouracil (**2**) (Fig. 1A) functionalized Ru(II)-polypyridyl derivatives having $\Delta\lambda$ s of $\sim 160 \text{ nm}$ for specific imaging of endoplasmic reticulum, cell membrane and cytoplasmic vacuoles, lipid dense regions in live MCF-7 cells. Both complexes showed insignificant cytotoxicity and a lipophilicity dependent cellular internalization process. Importantly, in fixed MCF-7 cells, localization of dyes **1** and **2** were observed only in nucleus and such observation is hitherto unknown. It is noteworthy that the model complex **3** ($[\text{Ru}(\text{bpy})_2(\text{L}_3)]^{2+}$; bpy = 2,2'-bipyridine & $\text{L}_3 = 4,4'$ -dimethyl-2,2'-bipyridine, Fig. 1C) did not show any such specificity either in live or in fixed MCF-7 cells.

Results and discussion

5-Fluorouracil (5-FU) and Uracil (U) are well known for their rapid cellular uptake.²³ With an aim to exploit this property two new uracil derivatives $[\text{Ru}(\text{bpy})_2(\text{L}_1)]^{2+}$ (**1**); and $[\text{Ru}(\text{bpy})_2(\text{L}_2)]^{2+}$ (**2**) were synthesized. The model complex $[\text{Ru}(\text{bpy})_2(\text{L}_3)]^{2+}$ (**3**) was also prepared for the comparison purpose. Selection of Cl^- as counter anions for **1**, **2**, and **3** enabled us to achieve the desired solubility in aq. buffer (Tris-HCl buffer, pH = 7.4) media. Synthetic methodology as well as various analytical and spectroscopic data ($^1\text{H}/^{19}\text{F}$ NMR and HRMS spectra) of complexes **1**(Cl)₂, **2**(Cl)₂, and **3**(Cl)₂ are discussed in supporting information (SI Figs. S7–S20). All these data agreed well for the desired purity of these complexes.

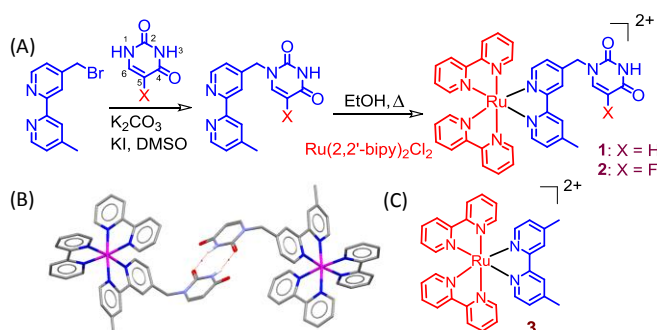


Fig. 1 (A) Synthetic route followed for achieving complexes **1** and **2**, (B) single crystal X-ray structure for complex **1**, (All hydrogen atoms, are omitted for clarity and for the same reason counter anions (PF_6^-) are also removed), (C) the molecular structure of the model complex **3**.

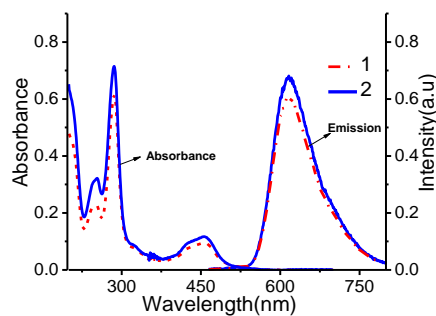


Fig. 2 Absorption and emission spectra of complexes **1** and **2** in aqueous medium.

Complex **1** was also characterized by single crystal X-ray structural analysis (ESI Table S1) Optical spectra for complexes **1** and **2** are shown in Fig. 2, which clearly revealed that the electronic spectra in the visible region for both complexes was dominated by broad metal-to-ligand charge-transfer (MLCT; $\text{Ru}(\text{d}\pi) \rightarrow \text{bpy}/\text{L}_1(\pi^*)$ and/or $\text{bpy}/\text{L}_2(\pi^*)$ based transitions at $\sim 455 \text{ nm}$, while emission band for respective complex was attributed to a $^3\text{MLCT}$ transition ($\sim 620 \text{ nm}$ for $\lambda_{\text{Ext}} = 455 \text{ nm}$) as the Φ_{ISC} for the ISC process for Ru(II)-polypyridyl complexes is reported to be ~ 1 and occur within 40 fs.²⁴ Spectroscopic data for complex **1**: $\lambda_{\text{Max}}^{\text{Abs}} = 287 \text{ nm}$, $\epsilon = 54740 \text{ M}^{-1}\text{cm}^{-1}$; $\lambda_{\text{Max}}^{\text{Abs}} = 457 \text{ nm}$, $\epsilon = 12920 \text{ M}^{-1}\text{cm}^{-1}$; $\lambda_{\text{Max}}^{\text{Ems}} = 620 \text{ nm}$ ($\Phi_{\text{Ems}} = 0.048$) for λ_{Ext} of 457 nm and $\tau_{1/2} = 323 \text{ ns}$ ($\chi^2 = 1.14$) using 442 nm laser source; Spectroscopic data for complex **2**: $\lambda_{\text{Max}}^{\text{Abs}} = 287 \text{ nm}$ ($\epsilon = 79350 \text{ M}^{-1}\text{cm}^{-1}$); $\lambda_{\text{Max}}^{\text{Abs}} = 456 \text{ nm}$, $\epsilon = 13850 \text{ M}^{-1}\text{cm}^{-1}$; $\lambda_{\text{Max}}^{\text{Abs}} = 617 \text{ nm}$ ($\Phi_{\text{Ems}} = 0.050$) for λ_{Ext} of 456 nm and $\tau_{1/2} = 336 \text{ ns}$ ($\chi^2 = 1.02$); Spectroscopic data for complex **3**: $\lambda_{\text{Max}}^{\text{Abs}} = 286 \text{ nm}$ ($\epsilon = 65350 \text{ M}^{-1}\text{cm}^{-1}$); $\lambda_{\text{Max}}^{\text{Abs}} = 453 \text{ nm}$, $\epsilon = 14250 \text{ M}^{-1}\text{cm}^{-1}$; $\lambda_{\text{Max}}^{\text{Abs}} = 616 \text{ nm}$ ($\Phi_{\text{Ems}} = 0.055$) for $\lambda_{\text{Ext}} = 453 \text{ nm}$ and $\tau_{1/2} = 321 \text{ ns}$ ($\chi^2 = 1.12$) using 442 nm laser source.

It can be assumed that the U and 5-FU permeate cell membrane using the facilitated transport mechanism and 5-FU remains the main reagent for the treatment of colorectal cancer.^{21,25} 5-FU is known to be converted to fluorodeoxyuridine monophosphate, which forms a stable complex with thymidylate synthase. This further inhibits deoxythymidine monophosphate production and interrupts the DNA synthesis.²⁶ However, the presence of $\text{N}^1\text{H}_{5\text{-FU}}$ is crucial for such action (Fig. 1A). Our synthetic design involved the removal of this N^1H with an aim to block its cytotoxicity as well as to avail the advantage of the cell membrane permeability.²⁷ Accordingly, complexes **1** and **2** were synthesized (Fig. 1A). Fig. 1B clearly reveals that the complex **1** exists as hydrogen bonded dimer in the solid state. Complex **3** was prepared as a model compound to investigate the role of U/5-FU in cell membrane permeability.

Isothermal titration calorimetry studies

Relative binding affinity of complexes **1**, **2**, and **3** towards calf-thymus DNA (CT-DNA) were evaluated using isothermal titration calorimetry (ITC) (Fig. 3). Association constants and thermodynamic parameters (Table. 1) clearly reveal that the

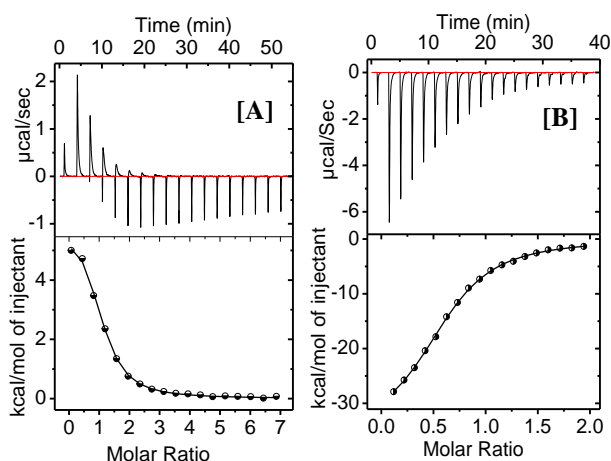


Fig. 3 ITC binding profiles for the interaction of (A) **1** and (B) **2** with CT-DNA at 25 °C in Tris-HCl buffer (pH=7.4).

Table 1. ITC-derived CT-DNA binding parameters for **1**, **2**, and **3**.

Complex	1	2	3
$K_s [M^{-1}]$	$(2.51 \pm 0.16)10^4$	$(7.23 \pm 0.24)10^4$	$(2.05 \pm 0.85)10^3$
$\Delta H [KcalM^{-1}]$	1.47 ± 0.02	-35.5 ± 0.41	0.51 ± 0.25
$-\Delta S [KcalM^{-1}]$	7.47	-28.87	5.03
$\Delta G [KcalM^{-1}]$	-6.0 ± 0.02	-6.68 ± 0.41	-4.52 ± 0.25
N [bp]	0.98 ± 0.01	0.61 ± 0.00	0.354 ± 0.14

binding affinities for complexes **1** and **2** are much higher than that of **3** towards CT-DNA.

The data shown in Table 1 clearly indicate that the affinities of these three complexes are much lower than those of analogous Ru(II)-polypyridyl derivatives having functionality which favour an efficient DNA intercalation process.²⁸ Complex **2** with 5-FU derivative was expected to be more lipophilic than the analogous complex **1** and anticipated to favour the interaction with DNA. Binding affinity of **2** towards CT-DNA was higher than the complex **1** by a factor of 2.9. A small positive enthalpy ($\Delta H_{ITC} = 1.47 \pm 0.02 \text{ Kcal.mol}^{-1}$) and a high positive entropy (7.47 Kcal M^{-1}) changes was observed for interaction of **1** with CT-DNA. These observations tend to suggest that the interaction of **1** with CT-DNA was entropically driven. The interaction of **2** with CT-DNA showed negative enthalpy ($\Delta H_{ITC} = -35.5 \text{ Kcal M}^{-1}$) and entropy changes ($-28.87 \text{ Kcal M}^{-1}$). High negative enthalpy change was anticipated, as fluorine containing compounds generally have higher solvation enthalpy. This also indicated that the interaction was enthalpically driven as well. A slight positive enthalpy ($\Delta H_{ITC} = 0.51 \pm 0.25 \text{ Kcal.mol}^{-1}$) and a positive entropy (5.03 Kcal M^{-1}) changes was observed for interaction of **3** with CT-DNA which is an entropically driven interaction (SI fig. S4). The binding affinity of all three complexes for the CT-DNA is **2** > **1** > **3**.

Our further studies also confirmed that none of these three complexes could alter the relative viscosities of aqueous DNA solutions (SI Fig. S6). All these observations suggested that **1**, **2**, and **3** could interact with CT-DNA predominantly through

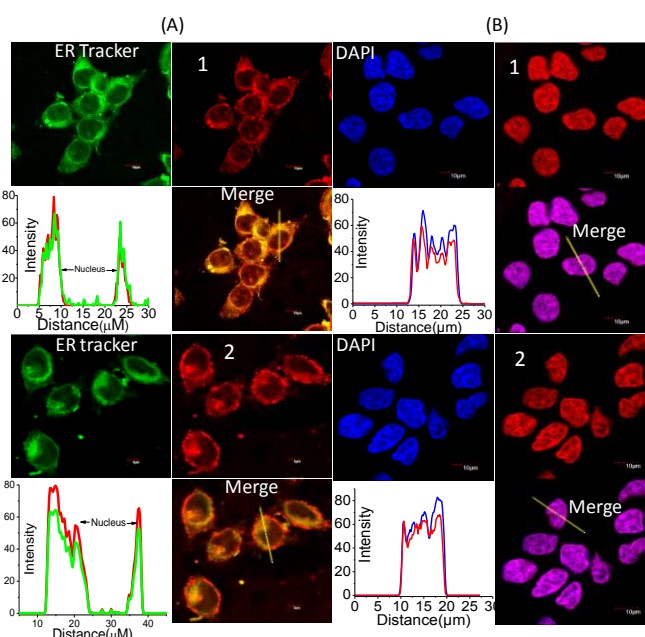


Fig. 4 CLSM images that shows the live cell uptake (A) and fixed cell staining (B) of **1** and **2**. Co-localization studies performed with ER-Tracker™ Green for live cells and with DAPI for fixed cells.

groove binding. However, certain trivial influence of the electrostatic interactions between these cationic complexes (**1**, **2**, and **3**) with the negatively charged phosphate backbone cannot be completely ruled out.

Cytotoxicity and cellular imaging studies

Cytotoxicity studies of complexes **1**, **2**, and **3** were investigated on MCF-7 cells using MTT (MTT = (3-(4,5-dimethylthiazol-2-yl)-2,5-diphenyltetrazolium bromide) assay methodology.[†] The cell viability was found to be $\geq 85\%$ after incubation with $300 \mu\text{M}$ of **1**, **2**, and **3** for 24 h. Thus, MTT assay confirmed that the insignificant toxicity of all three complexes towards MCF-7 cell lines (SI Fig. S5).[†] Evaluated IC₅₀ values were found to be $\geq 300 \mu\text{M}$.

Negligible toxicity towards MCF-7 cells encouraged us to explore their application potential as imaging agents and accordingly live MCF-7 cells were incubated separately with $50 \mu\text{M}$ of **1**, **2**, and **3** at $37 \text{ }^\circ\text{C}$. Close comparison of the confocal laser scanning microscopic (CLSM) images as well as the images of the co-staining experiments with well-known ER staining agent clearly revealed that intracellular emission for **1** and **2** were found to be exactly superimposed with those for ER-Tracker™ Green (Fig. 4A). Also, distinct emission of **1** and **2** was also observed from the cell membrane, indicating that the cell membrane was also a target for the reagents **1** and **2**. Identical studies with **3** did not show any such specificity towards lipid dense regions like ER or cell membrane (Fig. 6A). Also, the extent of cellular uptake for complex **3** was found to be less as compared to the reagents **1** and **2** (*vide infra*). The enlarged confocal images for reagents **1** and **2** (Fig. 5) revealed dot-like structures with red fluorescence in bright-

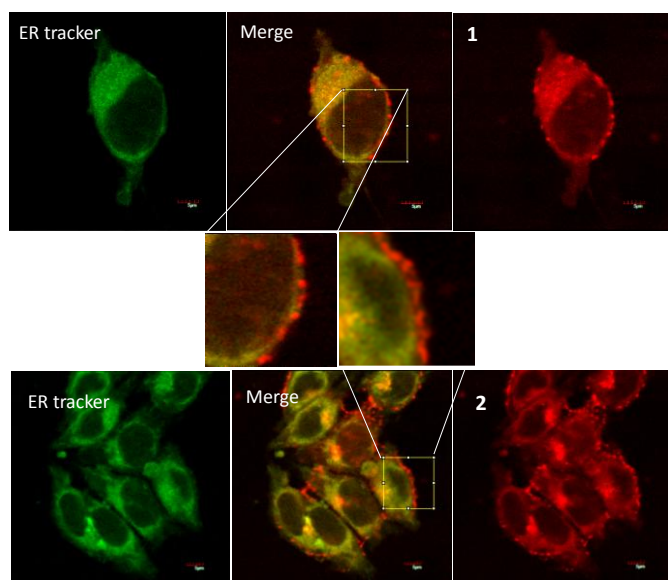


Fig. 5 CLSM images of cellular uptake of **1** and **2**. Colocalization experiments were performed using endoplasmic reticulum tracker (ER-Tracker Green (E34251)).

field microscopy, a pattern that is observed earlier for localization of lipophilic reagents at the cell membrane.²⁹ Such dot like structures scattered in the cytoplasm presumably suggested that the reagents were also sequestered in cytoplasmic vacuoles, which are known to play a subordinate role in endocytosis.^{30,31}

Partition coefficients ($\log P$) for these three complexes were evaluated by shake-flask method and these were correlated to the lipophilicity of respective complexes. Lipophilicity of the complexes **1** ($\log P = -0.85$), **2** ($\log P = -0.50$), and **3** ($\log P = -1.1$) were evaluated. These data clearly reveal that $\log P$ is the highest for complex **2** followed by **1** and **3**. There were some contrasting views in correlating the distinct role of lipophilicity and overall charge of the Ru(II)-polypyridyl derivatives to the cellular internalization. However, it has been argued by many research groups that lipophilicity of the reagent is more important than the overall charge of the cationic Ru(II)-complexes in influencing the cellular uptake process.^{20,21,31,34,35}

For our present study, all three complexes had the same overall charge (2+), while their lipophilicity followed the order **2** > **1** > **3**. Thus, one would presume that the cellular internalization would follow the order **2** > **1** > **3** and the experimental data are in accordance with the presumption (Table S2). This was further confirmed by the results of the MP-AES (Microwave Plasma Atomic Emission Spectroscopy) studies (SI Table S3). Fluorine substitution in complex **2** was used to improve the lipophilicity as compared to complex **1**. Thus, evaluated results were in good agreement with the trend described in the previous literature reports.³¹ The literature reports also reveal that more lipophilic cationic reagent are generally accumulated preferentially in the regions like ER, while analogous reagents having comparable overall charge and relatively lower lipophilicity would have preference for nuclei.^{13,14,36} Earlier reports reveal that internalization of Ru(II)-polypyridyl derivatives could occur through energy-dependent

and/or energy-independent processes.^{30,37,38} The cellular uptake of complexes **1** and **2** were found to be significantly reduced at lower temperature (4 °C vs. 37 °C; SI Fig. S21), which was consistent with energy-dependent transport.³⁹ This further suggested that the cellular uptake of complexes **1** and **2** presumably happened following an energy dependent endocytosis pathway.^{31,40,41} However, one could not completely rule out the possibilities of an adverse influence the reagent diffusion through the cell membrane due to reduced reagent solubility and decrease in cell membrane fluidity with lowering of temperature.

Literature reports reveal that the lipid bodies of cytoplasm in living cells are dynamic and their identification has methodological limitations, as lipid bodies dissipate upon drying or dissolve upon cell fixation.⁴² This clearly reveals that the fixation of cells using paraformaldehyde is expected to alter the subcellular distribution of internalized reagents. For example, some peptide-fluorophore conjugates have been shown to move from the cytoplasm to the nucleus following the fixation with formaldehyde.⁴³ To check such a possibility, we examined confocal laser scanning microscopic (CLSM) images of the PFA fixed MCF-7 cells after incubation with 50 μM of reagents **1** and **2**. Co-staining experiments were also performed with DAPI, a commonly used commercial nuclear staining agent. For cells treated with **1** and **2**, CLSM images were recorded following excitation with 442 nm laser and intra cellular emission of respective complexes were observed at 620 nm. Superimposed fluorescence intensity profile plots (Fig. 4B) of the intracellular emission signals of DAPI with those of **1** or **2**, confirmed that both reagents were as efficient as DAPI in staining the nucleus of the MCF-7 cells.

To examine the cellular uptake and staining properties of the analogous model complex **3**, we incubated the live MCF-7 cells with complex **3** for 4 h, and then imaged using confocal microscopy. The CLSM images revealed that unlike **1** and **2**, the non-specific internalization of **3** in live MCF-7 cells (Fig. 6A) was observed. Besides, the treatment of PFA fixed MCF-7 cells with **3** also resulted in non-specific staining of cellular compartments (Fig. 6B). Presumably, this could be attributed to the lack of the functional moieties (U/5-FU) and lower lipophilicity ($\log P = -1.1$) of complex **3**.

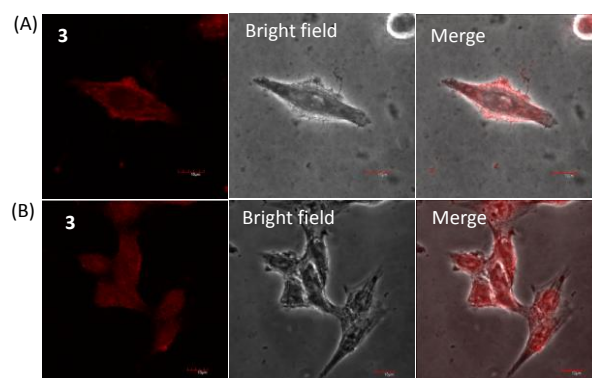


Fig. 6 CLSM images of MCF-7 cells that show the live cell uptake (A) and fixed cell staining (B) of complex **3**.

To ensure that DAPI had no influence in internalization of the reagents **1** and **2**, we had also performed identical experiments with fixed MCF-7 cells in absence of DAPI (SI Fig. S22) and a distinct red emission were observed from the nucleus. Luminescence intensity profile plots confirmed that the emission was actually from the nucleus.

In order to check the preferential binding of these two reagents to nuclear DNA, deoxyribonuclease (DNase I) and ribonuclease (RNase A) digest experiments were carried out. DNase I is an enzyme that catalyzes the hydrolytic cleavage of phosphodiester linkages in the DNA and RNase A is a type of nuclease that catalyzes the degradation of RNA into smaller components.⁴⁴ DAPI was used for control experiments. Comparison of the CLSM images of the cells pretreated with DNase I (Figs. 7(i) B & E) and RNase A (Figs. 7(i) C & F) clearly revealed that the intracellular fluorescence intensities of reagents **1** and **2** from the nucleus of MCF-7 cells were significantly reduced for cells that were pre-treated with DNase I and not for those pre-treated with RNase A. This confirmed that **1** and **2** are mainly targeting nuclear DNA in the fixed cell nucleus. To emphasize more on the specificity of complexes **1** and **2** binding to DNA, we synchronized the cells by treating with colchicine and released at different time points to obtain the cell cycle stages of prophase, metaphase, and telophase (Fig. 7(ii)). Clear staining of the DNA at various stages could be seen using complexes **1** and **2**.

Photostability test

We have also examined the photostability of these two dyes and compared with that for DAPI by using confocal microscopy (Fig. 8(i)) and fluorescence spectroscopy (Fig. 8(ii)). The fluorescence intensity of DAPI upon continuous irradiation in fixed MCF-7 cells (at 359 nm for 300 sec) was drastically reduced.

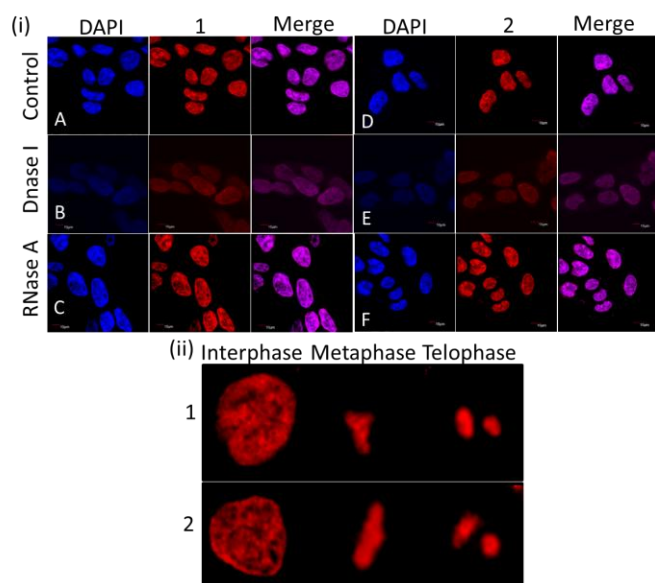


Fig. 7: CLSM images of MCF-7 cells stained with **1** (A-C) and **2** (D-F), (ii) CLSM images of MCF-7 cells during different stages of cell division using **1** and **2** as the cellular imaging agents.

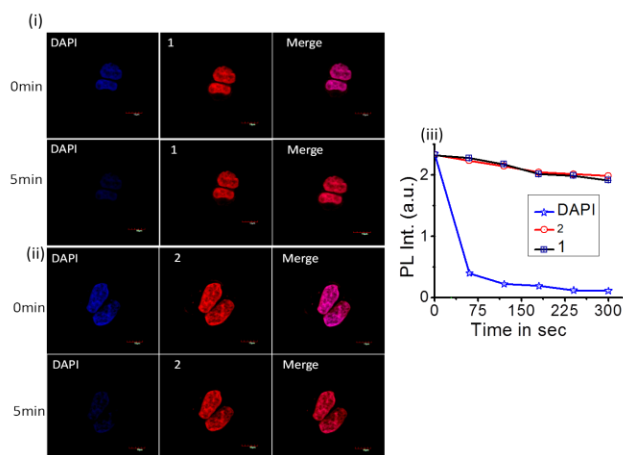


Fig. 8 Photostability test for **1**, **2**, and DAPI in MCF-7 cells by CLSM (i), (ii) and by fluorescence spectroscopy (iii).

In contrast, fluorescence intensity of **1** and **2** were only reduced by $\sim 20\%$ upon exposure at 442 nm for 300 sec, reflecting the photostability of these two fluorescent staining reagents. Despite remarkable stability and high emission quantum yield, the use of quantum dot material as imaging reagent is restricted owing to the high toxicity.⁴⁵⁻⁴⁷ Considering these features; the scope of visible light excitable reagents **1** and **2** with a $\Delta\lambda_{Ss}$ of ~ 160 nm is significant.

Conclusions

In conclusion, we have successfully developed two new U/5FU conjugated Ru(II)-complexes (**1** and **2**) as imaging reagents. Unlike model reagent **3**, both reagents were preferentially localized in lipid dense regions like ER, cell membrane, and cytoplasmic vacuoles of live MCF-7 cells. This illustrated the role of U/5FU functionality in achieving specificity for the lipid dense regions in live cells. Relatively higher lipophilicity of **2** helped in achieving better cellular internalization. For fixed cell, the lipid layer disruption helped in explicit localization in cell nucleus through specific interaction with cellular DNA. Insignificant toxicity, photo-stability, visible light excitation, and large $\Delta\lambda_{Ss}$ of ~ 160 nm are other key features for these two reagents and have significant characteristics for application as an imaging reagent.

Experimental section

General Information

All chemicals were purchased from Sigma Aldrich unless otherwise indicated. ¹H NMR spectra were recorded on a Bruker FT-NMR spectrometer at room temperature. ESI-MS measurements were carried out on a Waters QToF-Micro instrument. UV-Vis spectra were obtained by using a Cary 500 scan UV-Vis spectrometer. Complexes **1**, **2**, and **3** were converted into their water soluble chloride salts via anion metathesis. The CT-DNA concentration per nucleotide was determined by absorption spectroscopy by using the molar absorption coefficient ($6600 \text{ mol}^{-1} \text{ dm}^3 \text{ cm}^{-1}$) at 260 nm.

Physical Measurements

The emission spectra were obtained using Edinburgh instrument Xe-900 spectro fluorometer. Confocal microscopy images acquired using Olympus Fluoview microscope. Lifetimes were acquired using a Horiba TCSPC (Time Correlated Single Photon Counting) system exciting at 443 nm. 5,000 counts were collected for each lifetime measurement and all measurements were performed in triplicate using DAS software to confirm results. The calculation of the lifetimes was carried out with single exponential decay function to each decay plot to extract the lifetime information using DAS6 fluorescence decay analysis software. Partition coefficient (logP) measurements were calculated using shake-flask (n-octanol/water) method. The absorbance of respective complex in each phase was determined using UV-Vis spectroscopy. ITC experiments were performed with the Microcal iTC200. CT-DNA concentration (0.1 mmol) and complexes **1** (5 mmol), **2** (5 mmol) and **3** (5 mmol) concentrations were used for these experiments. All titrations were conducted in Tris-HCl buffer (5 mmol Tris and 25 mmol NaCl), pH = 7.4 at 25 °C. The resulting isotherms were fitted with the one set of site binding model provided with Microcal iTC200. MCF-7 cells were cultured in DMEM respectively supplemented with 10% FBS and penicillin/streptomycin. Cell lines were maintained at 37 °C in an atmosphere of 5% CO₂ and routinely sub-cultured. Cytotoxicity tests were performed using MTT assay. Metal accumulation studies for complexes **1**, **2**, and **3** were conducted on the MCF-7 cell line. The level of metal content in the cells was estimated using microwave plasma atomic emission spectroscopy.

Synthesis and characterization of **1**, **2**, and **3**

Two new uracil/5-fluorouracil derivatives [Ru(bpy)₂(L₁)]²⁺ (**1**); and [Ru(bpy)₂(L₂)]²⁺ (**2**); and (bpy = 2,2'-bipyridine) were synthesized. Model complex that was used for studies was [Ru(bpy)₂(L₃)]²⁺ (**3**) (where L₃ = 4,4'-dimethyl-2,2'-bipyridine). For complexes **1** and **2**, L₁ is 1-((4'-methyl-[2,2'-bipyridin]-4-yl)methyl)pyrimidine-2,4(1H,3H)-dione and L₂ = 5-fluoro-1-((4'-methyl-[2,2'-bipyridin]-4-yl)methyl) pyrimidine-2,4(1H,3H)-dione).

Synthesis of L₁ and L₂: The ligands L₁ and L₂ were prepared by alkylation of 4-(bromomethyl)-4'-methyl-2,2'-bipyridine in DMSO directly with uracil to give 1-((4'-methyl-[2,2'-bipyridin]-4-yl)methyl)pyrimidine-2,4(1H,3H)-dione(L₁) and with 5-fluorouracil at N¹ position to give 5-fluoro-1-((4'-methyl-[2,2'-bipyridin]-4-yl)methyl)pyrimidine-2,4(1H,3H)-dione(L₂),

Reaction of L₁ and L₂ with [Ru(bpy)₂Cl₂].xH₂O in ethanol for 8 h under reflux conditions afford a deep orange colored complexes **1** and **2** which were then purified by column chromatography (silica 100-200 mesh and 100% acetonitrile as eluent) and characterized using standard analytical techniques.

Note: Ligand L₃ (4,4'-dimethyl-2,2'-bipyridine) was obtained from Sigma-Aldrich and used without further purification for the synthesis of complex **3**.

Synthesis of (L₁) 1-((4'-methyl-[2,2'-bipyridin]-4-yl)methyl)pyrimidine-2,4(1H,3H)-dione: A mixture of uracil

(0.112 g, 1 mmol), K₂CO₃ (0.276 g, 2 mmol) and KI catalytic ca. 25 mg, a catalytic amount) in 10 mL of DMSO was stirred under N₂ for 10 min. 4-(bromomethyl)-4'-methyl-2,2'-bipyridine (0.644g, 2.45 mmol) predissolved in DMSO was then slowly added via a syringe and the resultant chocolate brown mixture was stirred under N₂ at room temperature for 3h. Water (100 mL) was then added and the suspension was extracted with dichloromethane. The collected organic layers were dried over anhydrous sodium sulphate and solvent was removed in vacuum to give a half-white solid. The crude was subjected to the silica column chromatography using dichloromethane and acetone as eluent 99:1 (v/v). The second spot on the TLC plate was collected as L₁: Yield: (0.145 g, 49.26%). ESI-MS: *m/z* = 316.91[L₁+Na⁺]; ¹H NMR (200MHz, MeOD) 8.65 (d, 1H, *J* = 5.7 Hz), 8.52 (d, 1H, *J* = 4.8 Hz), 8.24 – 8.18 (2H, m), 7.73 (d, 1H, *J* = 7.9 Hz), 7.38 (d, 1H, *J* = 3.4 Hz), 7.32 (d, 1H, *J* = 6.6 Hz), 5.77 (d, 1H, *J* = 7.9 Hz), 5.10 (2H, s), 2.49 (3H, s). Elemental analysis. Calcd: C, 65.30; H, 4.79; N, 19.04; Found: C, 64.9; H, 4.73; N, 18.98.

Synthesis of (L₂): 5-Fluoro-1-((4'-methyl-[2,2'-bipyridin]-4-yl)methyl)pyrimidine-2,4(1H,3H)-dione: A mixture of 5-fluorouracil (0.130 g, 1 mmol), K₂CO₃ (0.276 g, 2.0 mmol) and KI (ca. 25 mg) in 10 mL of DMSO was stirred under N₂ for 10 min. 4-(bromomethyl)-4'-methyl-2,2'-bipyridine (0.644 g, 2.45 mmol) predissolved in DMSO (5 mL) was then slowly added via a syringe and the resultant chocolate brown mixture was stirred under N₂ at room temperature for 3 h. Water (100 mL) was then added and the suspension was extracted with dichloromethane. The collected organic layers were dried over anhydrous sodium sulphate and the solvent removed in vacuum to give a half-white solid. The crude was subjected to the silica column chromatography using dichloromethane and acetone as solvent mixture 99:1 (v/v). The second spot from the bottom on the TLC plate was collected as L₂ (0.150 g, 48%) ESI-MS: *m/z* = 334.93[L₂+Na⁺]. ¹H NMR (200 MHz, CDCl₃) 8.89 (1H, s), 8.68 (d, 1H, *J* = 4.8 Hz), 8.54 (d, 1H, *J* = 4.8 Hz), 8.33 (1H, s), 8.25 (1H, s), 7.19 (d, 2H, *J* = 10.3 Hz), 5.77 (d, 1H, *J* = 7.7 Hz), 5.00 (2H, s), 2.45 (3H, s). ¹⁹F NMR(400 MHz, CDCl₃) - 74.85(1F, s). Elemental analysis. Calcd: C, 61.53; H, 4.20; N, 17.94; Found: C, 61.1; H, 4.14; N, 17.86.

Synthesis of [Ru(bpy)₂(L₁)](PF₆)₂ (1**), [Ru(bpy)₂(L₂)](PF₆)₂ (**2**) and [Ru(bpy)₂(L₃)](PF₆)₂ (**3**)**

Complexes **1**, **2**, and **3** were prepared using the reaction of [Ru(bpy)₂Cl₂]²⁺ (0.145 g, 0.3 mmol) with the appropriate ligand L₁(0.105 g, 0.3 mmol) or L₂(0.112 g, 0.3 mmol) or L₃(0.05 g, 0.3 mmol) in ethanol under reflux condition for 8 h. After cooling, addition of saturated aqueous potassium hexafluorophosphate (KPF₆) solution precipitated out the complexes as orange red solids. Which were filtered off using G4 glass cantered crucible. The precipitate washed with Millipore water (5x3 mL) followed by diethyl ether and dried over P₂O₅ in desiccator. Both the complexes were purified by silica gel (100-200 mesh) column chromatography using acetonitrile and saturated KPF₆ solution 98:2 (v/v) as eluent.

Characterization of **1:** (0.159 g, 53%), ESI-MS: *m/z* for M²⁺ = 707.1448 found, 707.1451 calculated, [M-2PF₆]⁺. ¹HNMR (400 MHz, CD₃CN) 9.26 (1H, s), 8.52 (4H, d, *J* = 8.0), 8.43 (1H, s),

8.34 (1H, s), 8.10-8.04 (4H, m), 7.75 (4H, d, $J = 4.5$), 7.69 (1H, d, $J = 5.8$), 7.57 (1H, d, $J = 5.7$), 7.49-7.39 (5H, m), 7.31-7.25 (2H, m), 5.70 (1H, d, $J = 7.8$), 5.05 (2H, s), 2.56 (3H, s). Elemental analysis (as chloride salt). Calcd: C, 55.53; H, 3.88; N, 14.39; Found: C, 55.41; H, 3.9; N, 14.4.

Characterization of 2: (0.165 g, 55%) ESI-MS: m/z for $M^{2+} = 725.1362$ found; 725.1357 calculated $[M-2PF_6]^+$. 1H NMR (500 MHz, CD_3CN) 9.52 (1H, s), 8.51 (4H, d, $J = 7.4$), 8.44 (1H, s), 8.31 (1H, s), 8.07 (4H, t, $J = 7.8$), 7.73 (4H, t, $J = 6.6$), 7.69 (1H, d, $J = 5.8$), 7.64 (1H, d, $J = 6.2$), 7.57 (1H, d, $J = 5.8$), 7.46-7.38 (4H, m), 7.32 (1H, d, $J = 5.4$), 7.27 (1H, d, $J = 5.6$), 5.01 (2H, s), 2.57 (3H, s). ^{19}F NMR (400MHz, CD_3CN) -168.99ppm. Elemental analysis (as chloride salt). Calcd: C, 54.28; H, 3.67; N, 14.07; Found: C, 54.2; H, 3.65; N, 13.96.

Characterization of 3: (0.151 g, 57%) ESI-MS: m/z for $M^{2+} = 299.07$. 1H NMR (200 MHz, CD_3CN) 8.58 (2H, s), 8.54 (2H, s), 8.43 (2H, s), 8.14-8.04 (4H, m), 7.80 (4H, d, $J = 5.6$), 7.60 (2H, d, $J = 5.8$), 7.50-7.40 (4H, m), 7.31-7.26 (2H, m), 2.57 (6H, s). Elemental analysis (as chloride salt). Calcd: C, 57.49; H, 4.22; N, 12.57; Found: C, 57.4; H, 4.2; N, 12.48.

Crystallographic Study of complex 1

As-synthesized crystal of complex **1** was obtained by slowly diffusion of Et_2O in to a CH_3NO_2 solution of complex **1**. The data collection was done at 298K. The crystal was mounted on a Super Nova Dual source X-ray diffractometer system (Agilent Technologies) equipped with a CCD area detector and operated at 250 W power (50 kV, 0.8 mA) to generate Mo $K\alpha$ radiation ($\lambda = 0.71073 \text{ \AA}$) and Cu $K\alpha$ radiation ($\lambda = 1.54178 \text{ \AA}$) at 298K. Data were integrated using CrysAlisPro software with a narrow frame algorithm. Data were subsequently corrected for absorption by the program SCALE3 ABSPACK1 scaling algorithm. Additional crystallographic data is available in supporting information.

Partition coefficient (logP) measurement

n-Octanol saturated water and water saturated octanol was obtained using Millipore water stirred with *n*-octanol for 24h before the two layers were separated by centrifugation (3000 rpm, 5 min). The chloride salts of complex **1**, **2**, and **3** were dissolved in *n*-octanol saturated water giving concentrations ranging from 0.5 to 3.0 mmol. This was then mixed with water saturated *n*-octanol in the ratio of 1:1 (v/v). Resulting solvent mixtures were vortexed for 30 min at room temperature and then were subjected to centrifugation (3000 rpm, 5 min) to get two separate layers. The absorbance of respective complex in each phase was determined using UV-Vis spectroscopy. The concentration in each phase was calculated using reference to calibration absorbance/concentration graphs in each phase and the octanol/water partition coefficient (logP) for **1**, **2**, and **3** was calculated using equation 1.^{48,49}

$$\text{LogP}_{\text{Oct/water}} = \log \left[\frac{(\text{complex})_{\text{Oct}}}{(\text{complex})_{\text{water}}} \right] \dots \dots \text{equation 1.}$$

Isothermal Titration Calorimetry (ITC) studies

ITC experiments were performed with the Microcal iTC200. CT-DNA concentration (0.1 mmol) and complexes **1** (5 mmol), **2** (5 mmol) and **3** (5 mmol) concentrations were used for these experiments. All titrations were conducted in Tris-HCl buffer (5 mmol Tris and 25 mmol NaCl), pH = 7.4 at 25 °C.⁵⁰ In each titration CT-DNA was loaded into the cell and complexes **1** or **2** or **3** were taken into the syringe. Aliquot of 2 μL of complexes were added to the cell containing DNA. In each experiment, the raw isotherms were corrected for heat of dilution by subtracting the isotherms representing the complexes injected into the Tris-HCl buffer. The resulting isotherms were fitted with the one set of site binding model provided with Microcal iTC200.

MTT assay and CLSM studies:

Cell cultures were treated with 0-300 μM solutions of **1**, **2** and **3** in triplicate for 24 h. After incubation 5 μL of MTT reagent was added and incubated for 4 h. MTT = (3-(4,5-dimethylthiazol-2-yl)-2,5-diphenyltetrazolium bromide) dissolved in serum-free media. The media was removed and the formazan dissolved using isopropanol and the absorbance at 570 nm quantified by plate reader (reference 620 nm). IC50 values for the entire three complexes were found to be >300 μM . MCF-7 cells were cultured in DMEM media. Cell lines were maintained at 37 °C in an atmosphere of 5% CO_2 and routinely sub-cultured. For CLSM, cell cultures were grown on 6 well plate with coverslips, after 24 h of incubation the cells were treated with solutions of **1**, **2**, and **3** (50 μM) in serum containing media and incubated for 4 h. After incubation media was removed and cells were washed with 1XPBS buffer. The cells were permeabilized using TritonX-100 followed by fixation with 4% paraformaldehyde and stained for confocal microscopy. Nuclear staining was performed by using DAPI. Endoplasmic reticulum staining studies were performed using ER tracker green (CAS No: E34251) from life technologies. For fixed cells, studies with complexes **1**, **2**, and **3** were performed after fixing the cells with 4% paraformaldehyde and treatment with 0.2% TritonX-100. To study different stages of mitosis, MCF-7 cells were seeded in coverslips and treated with 150 nM nocodazole for 14 h for mitosis arrest. Later nocodazole was removed and was supplemented in fresh complete DMEM medium. At 90th min after release from mitosis metaphase stage, cells were fixed with formaldehyde and stained for CLSM studies. At 160th min telophase stage of these cells collected were fixed with formaldehyde and stained for CLSM. Cells were fluorescently imaged on a Fluoview confocal laser scanning microscope by using 60X oil-immersion lenses. Complexes **1**, **2**, and **3** were excited with laser at 442 nm and emission monitored at 620 nm (red) wavelengths. DAPI was excited by using a 359 nm diode laser and emission detected with a 420-480 nm long-pass band-filter. ER tracker was excited at 504 nm.

Viscosity measurements

Viscosity studies were done in a Cannon-Manning semi micro viscometer (size 50) immersed in a thermostat bath maintained at 27 ± 1 °C. The concentration of Calf-thymus DNA was kept constant at 1 mmol and viscosity of the CT-DNA was measured by increasing the concentration of the ethidium bromide, **1**, **2**, and **3**. The flow times were measured after thermal equilibration of at least 30 min. Each sample was measured three times and the averaged time was used in calculations.^{51,52}

Cellular uptake & Quantification of **1**, **2**, and **3** by (MP-AES)

Cellular accumulation studies for complexes **1**, **2**, and **3** were conducted on the MCF-7 cell line. Briefly, 2.5×10^5 - 1×10^6 cells were seeded on a petridish; the metal complexes were then added to give final concentrations of 50 μ M and allowed a further 24 h of drug exposure at 37 °C. After this time, cells were treated with trypsin, counted using haemocytometer, and cells collected were digested overnight in concentrated nitric acid (73%) at 60 °C; Samples were made up to exactly 10 mL using deionized water and the amount of ruthenium taken up by the cells was estimated by MP-AES (Microwave Plasma Atomic Emission Spectroscopy), using an Agilent Technologies instrument (Model No: 4100 MP-AES). The solvent used for all MP-AES experiments was double deionized water (DDW). The concentrations used for the calibration curve were in all cases 0, 5, 7.5, 10 ppm. The isotope detected was ¹⁰¹Ru; readings were made in duplicate (N₂ gas mode).

Acknowledgements

AD acknowledges SERB (SB/S1/IC-23/2013) and CSIR-NCL (MLP028226) for financial support. VR and FA acknowledge BRNS and CSIR, respectively, for their fellowships.

Notes and references

- C. P. Montgomery, B. S. Murray, E. J. New, R. Pal and D. Parker, *Acc. Chem. Res.* 2009, **42**, 925–937.
- M. Terasaki, J. Song, J. R. Wong, M. J. Weiss and L. B. Chen, *Cell* 1984, **38**, 101-108.
- A. S. Boutorine, D. S. Novopashina, O. A. Krasheninina, K. Nozeret and A. G. Venyaminova, *Fluorescent probes for nucleic acid visualization in fixed and live cells*; 2013; Vol. **18**.
- M. Dailey, E. Manders, D. Soll and M. T Michael, *Handbook of Biol. Confocal Microsc.* 2006, 381-403.
- M. P. Coogan, V. Fernández-Moreira, J. B. Hess, S. J. A. Pope and C. Williams, *New J. Chem.* 2009, **33**, 1094-1099.
- A. J. Amoroso, M. P. Coogan, J. E. Dunne, V. Fernández-Moreira, J. B. Hess, A. J. Hayes, D. Lloyd, C. Millet, S. J. A. Pope and C. Williams, *Chem. Commun.* 2007, 3066-3068.
- V. Fernández-Moreira, F. L. Thorp-Greenwood and M. P. Coogan, *Chem. Commun.* 2010, **46**, 186-202.
- M. P. Coogan, P. J. Dyson and M. Bochmann, *Organometallics* 2012, **31**, 5671–5672.
- M. R. Gill, D. Cecchin, M. G. Walker, R. S. Mulla, G. Battaglia and J. A. Thomas, *Chem. Sci.* 2013, **4**, 4512-4519.
- J. P. Lu, Y. Wang, D. A. Sliter, M. M. P. Pearce and R. J. H. Wojcikiewicz, *J. Biol. Chem.* 2011, **286**, 24426-24433.
- S. Zhang, T. Wu, J. Fan, Z. Li, N. Jiang, J. Wang, B. Dou, S. Sun, F. Song and X. Peng, *Org. Biomol. Chem.* 2013, **11**, 555-558.
- J. R. Lakowicz, *Principles of Fluorescence Spectroscopy*, 3rd Ed. Springer.
- E. Baggaley, M. R. Gill, N. H. Green, D. Turton, I. V. Sazanovich, S. W. Botchway, C. Smythe, J. W. Haycock, J. A. Weinstein and J. A. Thomas, *Angew. Chem. Int. Ed.* 2014, **53**, 3367-3371.
- M. R. Gill, J. Garcia-Lara, S. J. Foster, C. Smythe, G. Battaglia, and J. A. Thomas, *Nat. Chem.* 2009, **1**, 662–667.
- M. R. Gill, D. Cecchin, M. G. Walker, R. S. Mulla, G. Battaglia, C. Smythe and J. A. Thomas, *Chem. Sci.* 2013, **4**, 4512-4519.
- F. R. Svensson, M. Matson, M. Li, and P. Lincoln, *Biophys. Chem.* 2010, **149**, 102-106.
- L. Blackmore, R. Moriarty, C. Dolan, K. Adamson, R. J. Forster, M. Devocelle, and T. E. Keyes, *Chem. Commun.* 2013, **49**, 2658-2660.
- C. A. Puckett and J. K. Barton, *J. Am. Chem. Soc.* 2009, **131**, 8738-8739.
- X. Li, A. K. Gorle, T. D. Ainsworth, K. Heimann, C. E. Woodward, J. Grant Collins and F. Richard Keene, *Dalton Trans.* 2015, **44**, 3594-3603.
- R. Cao, J. Jia, X. Ma, M. Zhou and H. Fei, *J. Med. Chem.* 2013, **56**, 3636-3644.
- F. R. Svensson, M. Abrahamsson, N. Strömberg, A. G. Ewing, and P. Lincoln, *J. Phys. Chem. Lett.* 2011, **2**, 397-401.
- X. Meng, M. L. Leyva, M. Jenny, I. Gross, S. Benosman, B. Fricker, S. Harlepp, P. Hébraud, A. Boos, P. Wlosik, P. Bischoff, C. Sirlin, M. Pfeffer, J. P. Loeffler and C. Gaiddon, *Cancer Res.* 2009, **69**, 5458-5466.
- R. M. Wohlhueter, R. S. McIvor and P. G. Plagemann, *J. Cell. Physiol.* 1980, **104**, 309-319.
- C. M. White, F. Gonzalez, D. A. Bardwell, L. H. Rees, J. C. Je, M. D. Ward, N. Armaroli, F. Barigelletti, I. Frae-cnr and V. P. Gobetti, *J. Chem. Soc. Dalton Trans.* 1997, 727-735.
- N. Armaroli, F. Barigelletti, G. Calogero, L. Flamigni, C. M. White and M. D. Ward, *Chem. Commun.* 1997, 2181-2182.
- A. C. Bhasikuttan, M. Suzuki, S. Nakashima and T. Okada, *J. Am. Chem. Soc.* 2002, **124**, 8398-8405.
- D. B. Longley, D. P. Harkin and P. G. Johnston, *Nat. Rev. Cancer.* 2003, **3**, 330-338.
- S. Farquharson, A. Gift, C. Shende, F. Inscore, B. Ordway, C. Farquharson and J. Murren, *Molecules.* 2008, **13**, 2608-2627.
- N. Zhang, Y. Yin, X. Jie Sheng and W. S. Chen, *Molecules.* 2008, **13**, 1551-1569.
- M. R. Gill and J. A. Thomas, *Chem. Soc. Rev.* 2012, **41**, 3179-3192.
- O. Zava, S. M. Zakeeruddin, C. Danelon, H. Vogel, M. Grätzel and P. J. Dyson, *Chembiochem.* 2009, **10**, 1796-1800.
- Y. Chen, W. Xu, J. Zuo, L. Ji and H. Chao, *J. Mater. Chem. B.* 2015, **3**, 3306-3314.
- C. Tan, S. Lai, S. Wu, S. Hu, L. Zhou, Y. Chen, M. Wang, Y. Zhu, W. Lian, W. Peng, L. Ji and A. Xu, *J. Med. Chem.* 2010, **53**, 7613-7624.
- V. Fernández-Moreira, F. L. Thorp-Greenwood, A. J. Amoroso, J. Cable, J. B. Court, V. Gray, A. J. Hayes, R. L. Jenkins, B. M. Kariuki, D. Lloyd, C. O. Millet, C. F. Williams and M. P. Coogan, *Org. Biomol. Chem.* 2010, **8**, 3888-3901.
- X. Liang, J. Mack, L.-M. Zheng, Z. Shen and N. Kobayashi, *Inorg. Chem.* 2014, **53**, 2797-2802.
- W. Xu, J. Zuo, L. Wang, L. Ji and H. Chao, *Chem. Commun.* 2014, **50**, 2123-2125.
- W. Cao, W. Zheng and T. Chen, *Sci. Rep.* 2015, **5**, 9157; DOI: 10.1038/SREP09157.
- T. Gunnlaugsson, S. M. Cloonan, R. Elmes, M. Erby, S. A. Bright, F. E. Poynton, D. E. Nolan, S. J. Quinn and D. C. Williams, *J. Med. Chem.* 2015, **58**, 4494-4505.
- G. Drin, S. Cottin, E. Blanc, A. R. Rees and J. Temsamani, *J. Biol. Chem.* 2003, **278**, 31192-31201.

- 40 M. P. Coogan and V. Fernández-Moreira, *Chem. Commun.* 2014, **50**, 384-399.
- 41 C. A. Puckett and J. K. Barton, *J. Am. Chem. Soc.* 2007, **129**, 46-47.
- 42 C. A. Puckett, R. J. Ernst and J. K. Barton, *Dalton Trans.* 2010, **39**, 1159-1170.
- 43 J. P. Richard, K. Melikov, E. Vives, C. Ramos, B. Verbeure, M. J. Gait, L. V. Chernomordik and B. Lebleu, *J. Biol. Chem.* 2003, **278**, 585-590.
- 44 S. Feng, K. Kim, Yang and Y. SiqiangChang, *Chem. Commun.* 2010, **46**, 436-438.
- 45 W. Liu, M. Howarth, A. B. Greytak, Y. Zheng, D. G. Nocera, A. Y. Ting and M. G. Bawendi, *J. Am. Chem. Soc.* 2008, **130**, 1274-1284.
- 46 C.-L. Huang, C.-C. Huang, F.-D. Mai, C.-L. Yen, S.-H. Tzing, H.-T. Hsieh, Y.-C. Ling and J.-Y. Chang, *J. Mater. Chem. B.* 2015, **3**, 651-664.
- 47 R. Gui, H. Jin, Z. Wang and L. Tan, *Coord. Chem. Rev.* 2015, **296**, 91-124.
- 48 K. Y. Zhang and K. K. W. Lo, *Inorg. Chem.* 2009, **48**, 6011-6025.
- 49 V. Ramu, M. R. Gill, P. J. Jarman, D. Turton, J. A. Thomas, A. Das, and C. Smythe, *Chem. Eur. J.* 2015, **21**, 9185-9197.
- 50 M. G. Walker, V. Gonzalez, E. Chekmeneva and J. A. Thomas, *Angew. Chem. Int. Ed.* 2012, **124**, 12273-12276.
- 51 M. Gill, H. Derrat, C. Smythe, G. Battaglia and J. A. Thomas, *ChemBiochem* 2011, **12**, 877-880.
- 52 A. Ghosh, A. Mandoli, D. K. Kumar, N. S. Yadav, T. Ghosh, B. Jha, J. A. Thomas, and A. Das, *Dalton Trans.* 2009, **42**, 9312-9321.